An Energy Efficient RF Backscatter Modulator for IoT Applications

Ryan Reed, Fariborz Lohrabi Pour, and Dong Sam Ha
Multifunctional Integrated Circuits and System (MICS) Group
Bradley Department of Electrical and Computer Engineering
Virginia Tech, Blacksburg, Virginia, 24061, USA
E-mail: {ryanreed, fariborzlp, ha} @vt.edu

***Abstract*—This paper presents a compact backscatter modulator tag operating at 1.76 GHz. The modulator is composed of a series combination of a variable resistor and a varactor. These components modulate the backscatter signal by adjusting the input impedance or input reflection coefficient. A gallium nitride (GaN) on silicon carbide (SiC) high electron mobility transistor (HEMT) is adopted to implement the variable resistor. The modulator can support a variety of modulation schemes without increasing the size and design complexity. The tag can be continuously powered through ambient RF energy in the 2.45 GHz frequency band. A differential rectifier harvests RF energy to power a microcontroller eliminating the need for a battery. Experimental results show that the modulator can support 16-QAM with an error vector magnitude (EVM) of 1.73%. The measured RF to DC power conversion efficiency (PCE) of the energy harvester is 57.1% at a received power of 1.7 dBm.**

Keywords— RF backscattering, RF energy harvesting, quadrature modulation, Internet of Things (IoT)

I. INTRODUCTION

Low-power communication methods will be a key component in the development of IoT technology. One promising communication method that is adopted in numerous commercial and industrial applications is backscattering. Backscattering systems, such as passive RFID tags, relay information by reflecting the received RF signals. This method can minimize power consumption as the RF signals do not need to be synthesized. A conventional backscattering communication system is shown in Fig 1 [1]. It consists of an antenna, a switch, and various loads.

The system in Fig. 1 requires a dedicated transmitter for the backscatter device to receive power and RF signals [2]. To address this problem, ambient backscattering communication systems (ABCs) are developed [2]-[10]. These devices can harvest energy from ambient RF sources and utilize the energy to power a backscattering circuit. These ambient RF sources include FM radio [11]-[13], DTV [14]-[15], cellular [16]-[19], or 2.4 GHz ISM band transmissions such as Wi-Fi [20]-[22].

Numerous publications present backscatter communication systems. Daskalakis et al. [3] developed an ambient FM backscattering system for agricultural applications. The system consist of a low power microcontroller, which toggles switches with different load impedances. A super capacitor charged through RF energy harvesting provides the power for the backscattering system. The device featured a low design complexity, but the simple ON-OFF modulation limits its data rate and is spectrally inefficient. Thomas et al. [4] developed a high bit rate, 16-QAM backscatter by utilizing four sets of single pole four throw (SP4T) switches. The drawbacks of the design are that switches take up a significant amount of space and are difficult to power solely through ambient RF energy. In another work, Daskalakis et al. [5] developed a low powered ambient backscattering transmitter that utilized 4 – PAM. The transmitter adopts an active load as the modulator, which is realized by a single RF transistor driven by a digital-to-analog converter (DAC). Four distinct impedance levels are achieved by modulating the gate voltage of the transistor. It would be challenging to employ higher order modulation because of transistors limited variation in the parasitic capacitances. Correia et al. also utilized transistors to develop a backscatter modulator [6]. The design adopts a dual band Wilkinson power divider to generate a 4-QAM modulation using ambient 900MHz and 2.45 GHz signals. By backscattering multiple frequencies, they achieved a high bit rate of 500kps. However multiple transmission frequencies complicate the receiver design.

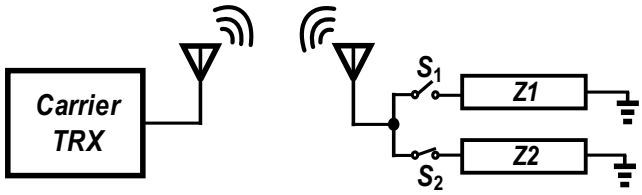

Fig. 1. Conventional RF backscattering system.

To address these shortcomings, this paper proposes a backscatter tag capable of high order QAM modulations. The device is capable of being powered by ambient RF energy and backscatters signals in the ambient GSM 1.8 GHz band. The tag utilizes a gallium nitride (GaN) on silicon carbide (SiC) high electron mobility transistor (HEMT) operating in the triode region, as well as a commercial-off-the-shelf (COTS) varactor to emulate district impedances. The varactor and transistor can be controlled by a low power microcontroller, which can be powered by the energy harvested by a 2.45 GHz rectifier.

This paper is organized as follows. Section II presents the design methodology, Section III shows the measured results and the paper is concluded in Section IV.

II. Design Methodology

A. Backscatter Tag Design

Backscatter QAM modulation is achieved by systematically adjusting the load impedance presented to antenna. A N-QAM I-Q constellation requires N number of load impedances [4] [23], where each symbol on the constellation can be expressed as

$$S_I = x_I + jy_Q \tag{1}$$

where x_I represents the in-phase component and y_Q represents the quadrature component for a given symbol, S_I. For the passive backscattering case, each symbol must be scaled to fit on the Smith chart [4]. This can be achieved by using the following expression

$$\Gamma_L = \alpha \frac{S_I}{\max|S_I|} \tag{2}$$

where α ranges from 0 to 1 and represents the scaling factor and Γ_L is the reflection for a given constellation point [24]. As α moves closer to 0, the constellation points move closer together on the Smith chart. This simplifies the circuit design, as fewer components are needed, and lower biasing ranges can be used. Having said this, large α values are desirable, as distant constellation points provide higher reflected powers to the intended receiver, increasing SNR [24]. It can be complicated to design a circuit that exhibits a large scaling factor with minimal complexity and biasing conditions.

The circuit presented in this paper achieves a scaling factor of 0.45. Fig. 2 shows the constellation diagram for 4, 16, and 64 QAM. The constellations are shifted to the right due to the channel resistance and capacitance range of the GaN HEMT and the varactor. This range also determines the scaling factor. The load impedances required to generate each constellation are calculated from the expression shown

$$Z_L = \frac{Z_0(1+\Gamma_L)}{1-\Gamma_L} \tag{3}$$

where Z_0 and Z_L represent the source impedance and load impedances, respectively. The source impedance is typically a 50 Ω antenna. Table I lists the required load impedances to cover the four-reflection coefficient at the corners of the constellation. These values correspond to the maximum and minimum values of the resistance and reactance. The impedance values in Table I are realized using a zero-biased Cree CGH40006P RF GaN HEMT as a variable resistor and the Skyworks 1248 varactor for its variable reactance [25]-[26].

A simplified, equivalent model for the GaN HEMT in the triode region, is shown in Fig. 3. The model is developed based on the Angelov model in triode region [27]. R_{eq} is the series combination of the parasitic resistances in the drain, source, and intrinsic channel of the transistor. L_D, L_S and C_{pd} are the parasitic inductances at the drain and the source and the pad capacitance, respectively. Fig. 4 (a) shows the resistive and reactive terms of the drain impedance for the selected GaN HEMT at 1.8 GHz. The real part is taken as the variable resistance and controlled through the gate bias voltage and the reactive part is absorbed to form the imaginary term in (1). As the gate bias voltage increases from -3V to -2V, the channel resistance ranges from 53 Ω to 8.9 Ω. The chosen GaN HEMT

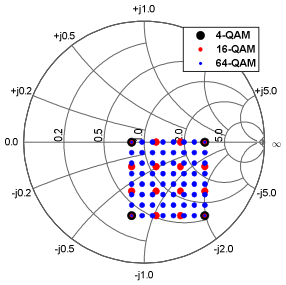

Fig. 2. Ideal 4, 16, and 64 QAM constellations.

TABLE I

Reflection and Impedance Values of Four Corners for 16-QAM with α = 0.45

#	Γ_L	Z_L
1	0.104 ∠ 180°	40.6 ∠ 0.923°
2	0.609 ∠ -99.7°	42.9 ∠ -62.3°
3	0.504 ∠ 0°	151 ∠1 .24°
4	0.783 ∠ -50.3°	104 ∠ -72.2°

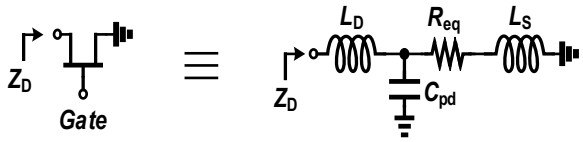

Fig. 3. Simplified equivalent model of GaN HEMT in triode region.

features a large range of resistances in the deep triode region with minimal changes in biasing in comparison to other RF transistors. This enables the modulator to support higher order modulation schemes while achieving relatively low error vector magnitude (EVM).

Keysight ADS simulations were conducted to simulate the backscatter modulator. The GaN HEMT model was obtained from the manufacture and proven accurate in previous works [28]-[30]. The large signal model of the varactor diode, including the parasitics of the package, was also used. Fig. 4 (b) shows the equivalent resistance and capacitance versus the control voltage applied across the varactor. As the applied reverse voltage increases from 0 to 5V, the capacitance of the varactor decreases from 22 pF to 1.49 pF, while its resistance decreases from 3.8 Ω to 1.8 Ω. When the transistor is operating near the cut off region ($V_{GS} \approx$ -3V) the varactor resistance is negligible. Fig. 5 shows the schematic of the backscatter transmitter where capacitors labeled as C_c are ac-coupling capacitors and inductors labeled as L_B are RF-chokes. The microstrip L-section at the input of the modulator is designed to shift Γ_L values to minimize the component biasing range, while achieving a sufficiently large range of impedance values.

B. Rectifier Design

The proposed 2.45 GHz rectifier is shown in Fig. 6. The topology consists of two voltage doublers with a differential output. With ideal diodes the voltage at the load should be approximately four times the voltage at the source input, the antenna [31]. Skyworks 7630 Schottky diodes are selected for the rectifier because of their low threshold voltage and series resistance [32].

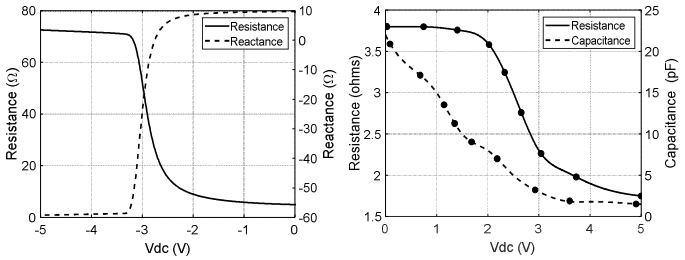

Fig. 4. (a) Resistive and reactive portion of GaN HEMT drain impedance and (b) measured resistance and capacitance of varactor.

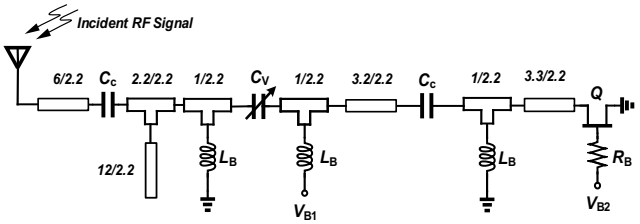

Fig. 5 Schematic of proposed backscatter with the dimensions (length/width) in mm.

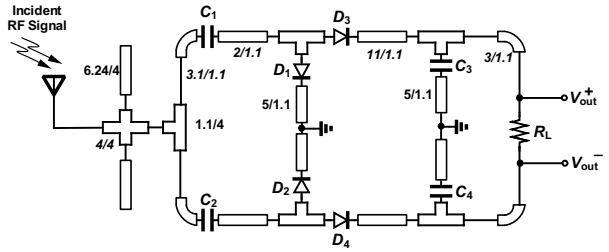

Fig. 6. Schematic of proposed energy harvester with the dimensions (length/width) in mm.

The ambient signals received by the energy harvester are typically weak. The Federal Communications Commission (FCC) limits the isotopically radiated power (EIRP) to 36 dBm in this band [33]. After propagation losses these signals are attenuated to approximately 10 dBm and -10 dBm for distances of 0.2 m and 2.5 m respectively, assuming a line of sight (LOS) link [33]. To ensure high RF to DC power conversion efficiency (PCE), the matching network should match the RF source to the rectifier at low input power. It enables the microcontroller to be powered by ambient RF energy. As the impedance of the rectifier can vary nonlinearly depending on the ambient power level, the source pull method is adopted for the input matching network, as described in [34]-[35]. The voltage doublers are connected after the T-branch matching structure using a power combiner. Simulation results show the loss of the power combiner to be 0.3 dB. The simulated large signal S_{11} parameter of the rectifier show that the developed matching network minimizes reflection for a wide input power range.

III. Measurement Results

The proposed energy harvester and backscatter modulator is assembled on a FR-4 (ε_r = 4.6) PCB substrate. The size of the complete system is 5.5 cm x 4.2 cm and has a thickness of 1.6 mm.

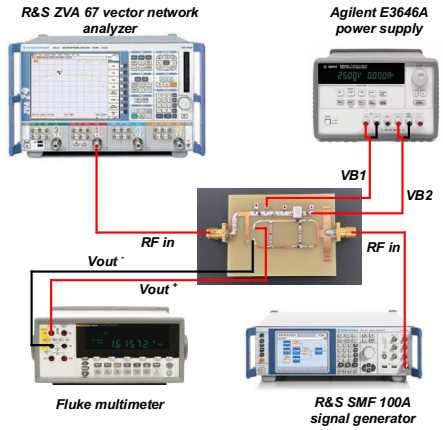

Fig. 7. Measurement setup for rectifier and backscatter measurements.

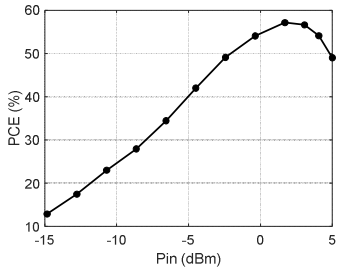

Fig. 8. Measured energy harvester PCE over input power range.

The test setup to measure the impedance states for a 16-QAM constellation and the RF to DC conversion efficiency of the rectifier is shown in Fig. 7. The R&S SMF 100A signal generator is used to model the ambient 2.45 GHz energy. The output power is measured at various resistive loads to find the peak efficiency. Fig. 8 shows the optimal rectifier measurement using a 4.5 kΩ load. The maximum PCE was 57.1% at the input power of 1.7 dBm. At this condition, the output voltage and current were determined to be 1.95 V and 0.433 mA, respectively. These conditions are sufficient to power a microcontroller. It should be noted that a tradeoff exists between maximum peak efficiency and efficiency at low input powers. The R&S ZVA 67 vector network analyzer was used to measure the impedance states for a 16-QAM constellation. The results are shown in Fig. 9 and is a close match to the ideal constellations.

Fig. 10 shows the resulting IQ constellation and indicates there is little fluctuation in the impedance states. The error vector magnitude (EVM) is obtained as 1.73% using (4). The EVM of the proposed backscatter is well below the 16-QAM modulator found in [4] with an EVM of 3.62%.

$$EVM = \sqrt{\frac{\frac{1}{N}\sum_{k=1}^{N}\left|S_{K_{Ideal}} - S_{K_{Measured}}\right|^2}{\max S_{Ideal}}} \qquad (4)$$

To achieve the constellation the HEMT gate biasing ranges varied from -4V to -1 V, and the reversed biased varactor voltage ranges from 0 to 5V range. The optimal backscattering frequency of 1.76 GHz was found as opposed to 1.8 GHz in simulations. This shift is reasonable and is a result of process variations.

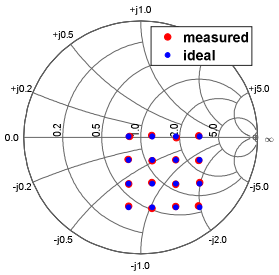

Fig. 9. Measured 16-QAM impedance states versus ideal constellation.

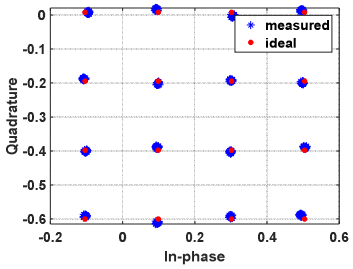

Fig. 10. Measured 16-QAM constellation in IQ plane.

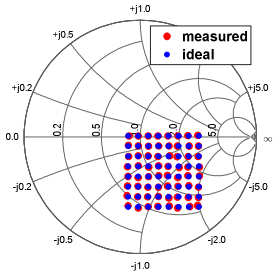

Fig. 11. Measured 64-QAM IQ constellation versus ideal constellation.

A major advantage of using a varactor and GaN HEMT, as opposed to fixed impedance switches, is the constellation can easily be altered to model different modulation complexities. EVM can also be minimized as the impedance can be adjusted. Fig. 11 shows a 64-QAM constellation for the proposed backscatter. Unlike the circuit in [4], the proposed backscatter can implement a different QAM constellation by adjusting the gate bias and varactor voltage. However, as the case with all backscattering systems, the increase in modulation order results in each point on the constellation being closer together. This can deteriorate the SNR and complicate the receiver design.

Fig. 12 shows a schematic diagram of the proposed backscatter with the bias voltage set up. A low power microcontroller with a DAC should be able to bias the varactor while the GaN HEMT can be biased using a DAC and a level shifter. To obtain the negative voltages required to bias the GaN HEMT the negative differential port of the energy harvester can provide a reference voltage for the level shifter.

Table II compares the proposed backscatter system to prior works. Unless noted otherwise, the energy/bit for each work was determined by dividing the power consumption by the bit rate. This work achieved a low energy/bit using a 64 QAM modulation scheme.

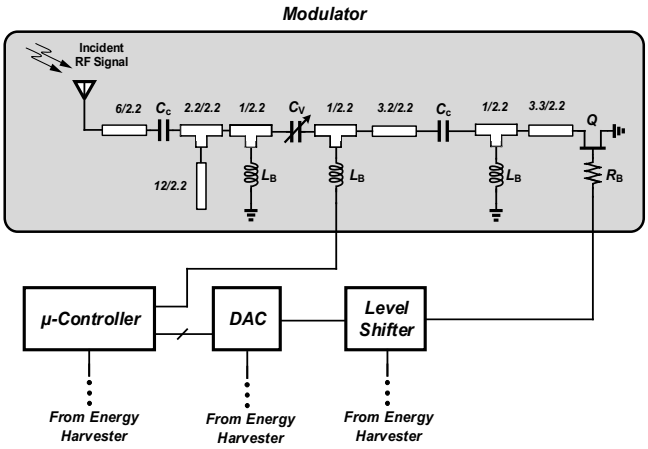

Fig. 12. Complete biasing setup for the proposed backscatter tag.

In this work the power consumption of the modulator was estimated by measuring the simulated DC power consumption in Keysight ADS. It was found that the GaN HEMT and varactor dissipated 2.06 uW at a symbol rate of 16 Mbps. From these results, it can be estimated that the modulator would exhibit an energy per bit rate of 21.4 fJ/bit using a 64 QAM modulation with a total bit rate of 96 Mbps.

TABLE II: COMPARISON BETWEEN PRIOR WORKS

Work	[3]	[4]	[5]	[6]	This Work
Modulation	ASK	16-QAM	4-PAM	4-QAM	Up to 64 QAM
Frequency	FM band	915 MHz	FM band	900 MHz and 2.45 GHz	1.76 GHz
RF powered compatible	Yes	No	Yes	Yes	Yes
Bit rate	500 bps	96 Mbps	10.2 kbps	500 kbps	96 Mbps
Energy/bit	NA	15.5pJ/bit†	27.7 nJ/bit*	54fJ/bit†	21.4 fJ/bit†

*Includes power consumption of control unit.
†Excludes power consumption of control unit.

IV. CONCLUSION

This paper presents a 1.76 GHz backscattering tag that can be powered of a 2.45 GHz RF energy harvester. A key advantage of the proposed tag over the switch-based works is the ability to select the optimal QAM constellation through adjustment of bias voltages. The varactor and a GaN HEMT acting in the triode region are used for this purpose. Measurement results show the proposed tag can switch from 16-QAM to 64-QAM readily and achieves a low EVM of 1.73%

ACKNOWLEDGMENT

This research was supported in part by the National Science Foundation Award no. 1814477

REFERENCES

[1] D. T. Hoang, D. Niyato, D. I. Kim, N. V. Huynh, and S. Gong, Ambient Backscatter Communication Networks. Cambridge: Cambridge University Press, 2020.

[2] U. N. Van Huynh, D. T. Hoang, X. Lu, D. Niyato, P. Wang and D. I. Kim, "Ambient Backscatter Communications: A Contemporary Survey," in IEEE Communications Surveys & Tutorials, vol. 20, no. 4, pp. 2889-2922, Fourthquarter 2018.

[3] S. Daskalakis, J. Kimionis, A. Collado, M. M. Tentzeris and A. Georgiadis, "Ambient FM backscattering for smart agricultural monitoring," 2017 IEEE MTT-S International Microwave Symposium (IMS), Honolulu, HI, pp. 1339-1341, 2017.

[4] S. J. Thomas and M. S. Reynolds, "A 96 Mbit/sec, 15.5 pJ/bit 16-QAM modulator for UHF backscatter communication," 2012 IEEE International Conference on RFID (RFID), pp. 185-190. Orlando, FL, 2012.

[5] S. N. Daskalakis, R. Correia, G. Goussetis, M. M. Tentzeris, N. B. Carvalho and A. Georgiadis, "Four-PAM Modulation of Ambient FM Backscattering for Spectrally Efficient Low-Power Applications," in IEEE Transactions on Microwave Theory and Techniques, vol. 66, no. 12, pp. 5909-5921, Dec. 2018.

[6] Correia and N. B. Carvalho, "Dual-Band High Order Modulation Ambient Backscatter," *2018 IEEE/MTT-S International Microwave Symposium - IMS*, Philadelphia, pp. 270-273, PA, 2018.

[7] J. Rosenthal and M. S. Reynolds, "A 158 pJ/bit 1.0 Mbps Bluetooth Low Energy (BLE) Compatible Backscatter Communication System for Wireless Sensing," 2019 IEEE Topical Conference on Wireless Sensors and Sensor Networks (WiSNet), Orlando, FL, USA, pp. 1-3, 2019.

[8] Y. Kim, C. Yoon, H. Ahn and S. Lim, "Implementation of Multi-level Modulated-Backscatter Communication System Using Ambient Wi-Fi Signal," 2019 IEEE International Conference on RFID Technology and Applications (RFID-TA), Pisa, Italy, pp. 1-3, 2019.

[9] T. A. Siddiqui, J. Holopainen and V. Viikari, "Ambient Backscattering Transponder With Independently Switchable Rx and Tx Antennas," in IEEE Sensors Letters, vol. 3, no. 5, pp. 1-4, May 2019.

[10] G. Vougioukas and A. Bletsas, "24μ Watt 26m range batteryless backscatter sensors with FM remodulation and selection diversity," 2017 IEEE International Conference on RFID Technology & Application (RFID-TA), pp. 237-242, Warsaw, 2017.

[11] E. M. Jung et al., "A Wideband, Quasi-Isotropic, Kilometer-Range FM Energy Harvester for Perpetual IoT," in IEEE Microwave and Wireless Components Letters, vol. 30, no. 2, pp. 201-204, Feb. 2020.

[12] S. Daskalakis, A. Georgiadis, A. Bletsas and C. Kalialakis, "Dual band RF harvesting with low-cost lossy substrate for low-power supply system," 2016 10th European Conference on Antennas and Propagation (EuCAP), Davos, Switzerland, pp. 1-4, 2016.

[13] N. Shariati, W. S. T. Rowe and K. Ghorbani, "Highly sensitive FM frequency scavenger integrated in building materials," 2015 European Microwave Conference (EuMC), Paris, France, 2015, pp. 68-71, doi: 10.1109/EuMC.2015.7345701.

[14] M. Piñuela, P. D. Mitcheson and S. Lucyszyn, "Ambient RF Energy Harvesting in Urban and Semi-Urban Environments," in IEEE Transactions on Microwave Theory and Techniques, vol. 61, no. 7, pp. 2715-2726, July 2013.

[15] S. Keyrouz, H. J. Visser and A. G. Tijhuis, "Ambient RF energy harvesting from DTV stations," 2012 Loughborough Antennas & Propagation Conference (LAPC), Loughborough, UK, , pp. 1-4, 2012.

[16] C. Song et al., "A Novel Six-Band Dual CP Rectenna Using Improved Impedance Matching Technique for Ambient RF Energy Harvesting," in IEEE Transactions on Antennas and Propagation, vol. 64, no. 7, pp. 3160-3171, July 2016.

[17] S. Shen, Y. Zhang, C. Chiu and R. Murch, "An Ambient RF Energy Harvesting System Where the Number of Antenna Ports is Dependent on Frequency," in IEEE Transactions on Microwave Theory and Techniques, vol. 67, no. 9, pp. 3821-3832, Sept. 2019.

[18] H. Tafekirt, J. Pelegri-Sebastia, A. Bouajaj and B. M. Reda, "A Sensitive Triple-Band Rectifier for Energy Harvesting Applications," in IEEE Access,vol.8, pp. 73659-73664, 2020.

[19] U. Muncuk, K. Alemdar, J. D. Sarode and K. R. Chowdhury, "Multiband Ambient RF Energy Harvesting Circuit Design for Enabling Batteryless Sensors and IoT," in IEEE Internet of Things Journal, vol. 5, no. 4, pp. 2700-2714, Aug. 2018.

[20] K. J. P. Jimenez, J. A. Hora, O. J. L. Gerasta, X. Zhu and E. Dutkiewicz, "Self-Biased 2.4 GHz CMOS RF-to-DC Converter with 80% Efficiency and −22.04 dBm Sensitivity for Wi-Fi Energy Harvesting," 2019 IEEE International Circuits and Systems Symposium (ICSyS), Kuantan, Pahang,Malaysia, pp. 1-4, 2019.

[21] E. V. V. Cambero, H. P. da Paz, V. S. da Silva, H. X. de Araújo, I. R. S. Casella and C. E. Capovilla, "A 2.4 GHz Rectenna Based on a Solar Cell Antenna Array," in IEEE Antennas and Wireless Propagation Letters, vol. 18, no. 12, pp. 2716-2720, Dec. 2019.

[22] K. R. Sadagopan, J. Kang, Y. Ramadass and A. Natarajan, "A cm-Scale 2.4-GHz Wireless Energy Harvester With NanoWatt Boost Converter and Antenna-Rectifier Resonance for WiFi Powering of Sensor Nodes," in IEEE Journal of Solid-State Circuits, vol. 53, no. 12, pp. 3396-3406, Dec. 2018.

[23] S. Thomas and M. S. Reynolds, "QAM backscatter for passive UHF RFID tags," 2010 IEEE International Conference on RFID (IEEE RFID 2010), Orlando, FL, USA, pp. 1-3, 2010.

[24] S. J. Thomas, E. Wheeler, J. Teizer and M. S. Reynolds, "Quadrature Amplitude Modulated Backscatter in Passive and Semipassive UHF RFID Systems," in IEEE Transactions on Microwave Theory and Techniques, vol. 60, no. 4, pp. 1175-1182, April 2012.

[25] Cree Inc. "CGH40006P 6 W, RF Power GaN HEMT" in Cree Wolfspeed Datasheet, 2020.

[26] Skyworks Inc., "SMVA1248-079LF: Hyperabrupt Junction Tuning Varactor," in Skyworks Datasheet, 2018.J. A. Hagerty, F. B. Helmbrecht, W. H. McCalpin, R. Zane and Z. B. Popovic.

[27] I. Angelov, K. Andersson, D. Schreurs, D. Xiao, N. Rorsman1, V. Desmaris, M. Sudow, and H. Zirath, "Large-signal modelling and comparison of AlGaN/GaN HEMTs and SiC MESFETs," in *Proc. Asia-Pacific Microwave Conf.*, 2006, pp. 279–282, Dec. 2006.

[28] S. Lee, S. Jeon and J. Jeong, "Harmonic-Tuned High Efficiency RF Oscillator Using GaN HEMTs," in IEEE Microwave and Wireless Components Letters, vol. 22, no. 6, pp. 318-320, June 2012.

[29] J. Moon, J. Lee, R. S. Pengelly, R. Baker and B. Kim, "Highly Efficient Saturated Power Amplifier," in IEEE Microwave Magazine, vol. 13, no. 1, pp. 125-131, Jan.-Feb. 2012.

[30] S. Kim, H. Kim, S. Shin, J. Kim, B. Kim and J. Choi, "Combined power oscillator using GaN HEMT," 2011 IEEE MTT-S International Microwave Symposium, Baltimore, MD, USA , pp. 1-1, 2011.

[31] J. -. Curty, N. Joehl, F. Krummenacher, C. Dehollain and M. J. Declercq, "A model for u-power rectifier analysis and design," in IEEE Transactions on Circuits and Systems I: Regular Papers, vol. 52, no. 12, pp. 2771-2779, Dec. 2005.

[32] Skyworks Inc., " Surface-Mount Mixer and Detector Schottky Diodes, SMS7630 series," in Skyworks Datasheet, 2019.

[33] M. ur Rehman, W. Ahmad and W. T. Khan, "Highly efficient dual band 2.45/5.85 GHz rectifier for RF energy harvesting applications in ISM band," 2017 IEEE Asia Pacific Microwave Conference (APMC), Kuala Lumpar, pp. 150-153, 2017.

[34] R. Reed, F. L. Pour and D. S. Ha, "An Efficient 2.4 GHz Differential Rectenna for Radio Frequency Energy Harvesting," 2020 IEEE 63rd International Midwest Symposium on Circuits and Systems (MWSCAS), Springfield, MA, USA, 2020, pp. 208-212.

[35] J. A. Hagerty, F. B. Helmbrecht, W. H. McCalpin, R. Zane and Z. B. Popovic, "Recycling ambient microwave energy with broad-band rectenna arrays," in IEEE Transactions on Microwave Theory and Techniques, vol. 52, no. 3, pp. 1014-1024, March 2004.